



http://pubs.acs.org/journal/acsodf Article

A Comprehensive Study of the Bridge Site and Substrate Relaxation Asymmetry for Methanethiol Adsorption on Au(111) at Low Coverage

Soumya Bhattacharya, Gil Speyer, David K. Ferry, and Lloyd A. Bumm*



Cite This: ACS Omega 2020, 5, 20874-20881



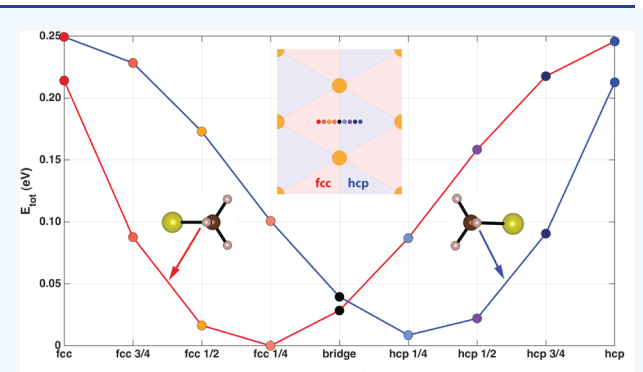
ACCESS I

III Metrics & More

Article Recommendations

s Supporting Information

ABSTRACT: We use dispersion-corrected density functional theory to explore the bridge-site asymmetry for methanethiol adsorbed on Au(111) with two different S–C bond orientations. We attribute the asymmetry to the intrinsic character of the Au(111) surface rather than the adsorbate. The preference for bridge-fcc versus bridge-hcp SCH₃ adsorption sites is controlled by the S–C bond orientation. The system energy difference favors the bridge-fcc site by 8.1 meV on the unrelaxed Au(111) surface. Relaxing the Au substrate increased this energy difference to 26.1 meV. This asymmetry is also reflected in the atomic displacement of the relaxed Au surface. Although in both cases, the bridge-site Au atoms shift away from the fcc 3-fold hollow site, the motion is greater for the bridge-fcc allowing a more favorable geometry for the sulfur atom to bond to the bridging atoms. We confirm that the adsorption energy is strongly dependent on the



inherent bridge-site asymmetry amplified 3x by substrate relaxation

S-C bond orientation and position, which can be understood in terms of a simple coordination geometry model. This work has important implications for alkanethiol surface diffusion and the structure of their self-assembled monolayers.

INTRODUCTION

Self-assembled monolayers (SAMs) of the *n*-alkanethiols on Au(111) have been intensively studied in the last 35 years^{1,2} for their diverse applications, primarily in electronics,³ surface modification,⁴ nanotechnology,⁵ and chemical sensing.⁶ A detailed understanding of the three regions of the SAM (Au/S interface, molecular backbone, and molecule/air interface) is important to better control the SAM structure for its applications.⁵ Both experimental and simulation techniques have been used to study the structure of the SAMs and to understand the influence of the structure on the SAM properties.^{7,8} The Au/S interface is the least understood part of SAMs compared to the other two regions. There is no general agreement regarding the atomic structure of the Au/S interface beyond the basic $(2\sqrt{3} \times 3)$ rectangular symmetry. Several Au/S interface models have been proposed, but none of them satisfy all the experimental observations. 14,15 Density functional theory (DFT) studies have found the bridge-fcc site and the staple motif to be the two most energetically favorable adsorption structures on the Au(111) substrate. The staple motif requires complex reconstruction of the substrate that involves adatoms, 19,20 while the bridge site does not. 16 In our work, we focus our discussion on the simpler bridge site and the resultant substrate relaxation in the absence of complex substrate reconstruction. Our motivation is to better understand the

azimuthal orientation of the S–C bond, which influences the alkyl chain packing in SAMs. Throughout our discussion, we adopt the convention of referring to the adsorbate by the precursor, methanethiol. This sidesteps assignment of the chemical nature of the adsorbate, which can have characteristics spanning a thiyl (radical) to a thiolate (anion). 9,22

The minimum energy position of the thiol S atom for adsorption at the bridge site is offset from the bridge site toward the fcc 3-fold hollow site (bridge-fcc) with the S–C bond azimuth toward the hcp 3-fold hollow site (hereafter, hcp-oriented). A second analogous minimum occurs on the opposite side at the bridge-hcp site with the S–C bond azimuth toward the fcc 3-fold hollow site (hereafter, fcc-oriented). Previous studies of these two sites found the bridge-hcp site to be 30 meV less favorable than the bridge-fcc site. In our work, we find a slightly smaller energy difference of 26.1 meV, which we presume is due to inclusion of the dispersion correction. The asymmetry between these sites extends beyond the orientation of the S–C bond. The bonding at the S atom

Received: May 18, 2020 Accepted: July 28, 2020 Published: August 13, 2020





was also found to be asymmetric as indicated by the different polar angles of the S–C bond—the angle between the surface normal and the S–C bond, 43.2° for the bridge-fcc site and 51.3° for the bridge-hcp site. ¹⁶ Because the energy difference between these two sites is on the order of kT at room temperature, both sites could be candidates for the SAM Au/S interface or play a role in SAM growth and surface diffusion. In this paper, we study the effect of the substrate relaxation on the asymmetry of the bridge-fcc and bridge-hcp sites.

The bridge site is one of the simple adsorption sites on the Au(111) substrate. The top-down view of a bridge-adsorbed sulfur atom is shown in Figure 1. The sulfur atom is bonded to

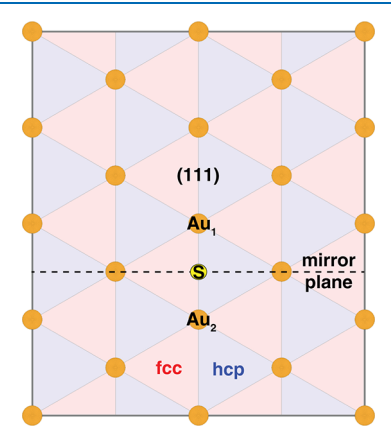


Figure 1. Top-down view of the simulation box showing the bridge site studied with an adsorbed S on Au(111). The S atom is on the mirror plane (dashed line) provided by the bridge site. The top layer Au atoms are shown here. The fcc and hcp 3-fold hollow sites are identified by the red and blue triangles, respectively. The S atom is bonded to the substrate via Au₁ and Au₂ bridging atoms. The crystallographic directions are shown on the edge of the unit cell (gray border) along with the coordinate system used for the DFT computations. Specifically, the crystallographic [112] direction is aligned with the DFT +x coordinate direction, the [110] with +y, and the [111] with +z.

two surface Au atoms (Au₁ and Au₂) along the $[\overline{1}10]$ direction. In the perpendicular $[11\overline{2}]$ direction, the fcc 3-fold hollow site

is to the left of the bridge site and the hcp 3-fold hollow site is to the right, denoted by the red and blue triangles, respectively. The bridge site does not have a mirror plane along the $[\overline{1}10]$ or a C_2 axis because the fcc and hcp 3-fold hollow sites are symmetry inequivalent (fcc-hcp asymmetry). However, the bridge site has a mirror plane parallel to the $[11\overline{2}]$ direction (bridge-site mirror plane) such that Au_1 and Au_2 are symmetry equivalent. We examine the bridge-site mirror plane symmetry during the substrate relaxation and find that the symmetry is preserved for the bridge-fcc site and approximately preserved for the bridge-hcp site.

The effect of the substrate relaxation on the asymmetry of these two sites has not been previously studied. We have chosen methanethiol as the adsorbate to explore the substrate relaxation for bridge-fcc and bridge-hcp adsorption sites. In this paper, we study the asymmetry of the adsorption energy for two S–C bond orientations on the unrelaxed and relaxed Au(111) surfaces. We first explore the asymmetry of the adsorption energy on the position of the adsorption site along the line through the bridge site between the fcc and hcp 3-fold hollow sites. Then, we study the relaxation of the bare Au(111) substrate followed by the relaxation induced by the methanethiol initially adsorbed at the bridge site as it relaxed into the bridge-fcc and bridge-hcp sites.

■ RESULTS AND DISCUSSION

Before looking at the Au surface relaxation, we get a picture of the inherent bridge-site asymmetry by studying the position-dependent adsorption energy on unrelaxed Au. Then, using the bare Au relaxation as our baseline, we compare the additional asymmetry induced through the substrate relaxation for the minimized energy bridge-fcc and bridge-hcp sites. Finally, we compare the molecular geometry to further analyze the asymmetry between the bridge-fcc and bridge-hcp sites.

We consider two sets of simulations to probe the inherent fcc-hcp asymmetry of the bridge site on unrelaxed Au(111) and the effect of the S–C bond orientation. We study the system energy of the adsorption sites at discrete positions along a path from the fcc 3-fold hollow site to the hcp 3-fold hollow site through the bridge site on the unrelaxed substrate

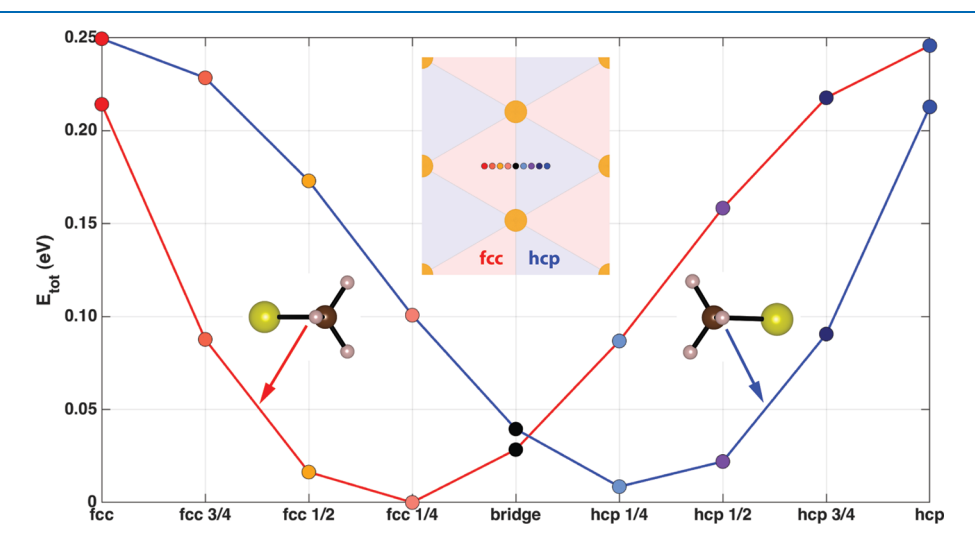


Figure 2. Energy for adsorption sites along the path from the fcc 3-fold hollow site to the hcp 3-fold hollow site for two orientations of the S–C bond is shown. Color-coded adsorption sites are shown in the inset. The energy shows strong dependence on the S–C bond orientation. The most stable configuration is the fcc-1/4. The hcp-1/4 is 8.5 meV less favorable than the fcc-1/4.

(Figure 2). One set is with the S-C bond hcp-oriented (red line) and the other with the S-C bond fcc-oriented (blue line). Each set shows a single minimum on opposite sides of the bridge site. The lowest energy in this series is achieved with the S-C bond being hcp-oriented and the S atom displaced from the bridge site toward the fcc 3-fold hollow site by 1/4 of the distance between the bridge and hollow sites (fcc-1/4). The equivalent lowest energy position with the S-C bond fccoriented and the S atom displaced from the bridge site toward the hcp 3-fold hollow site by 1/4 of the distance between the bridge and hollow sites (hcp-1/4). The fcc-1/4 is favored over the hcp-1/4 by 8.5 meV. In this series, both sites are very close to the energy-minimized structures obtained when the system is allowed to relax without constraints: the bridge-fcc and bridge-hcp. When the S atom is allowed to optimize its position on the surface, the system finds the bottom of these two curves where the energy difference between the bridge-fcc and bridge-hcp reduces to 8.1 meV (Table 1). The energy

Table 1. Comparison of the System Energy for the Energy-Minimized Structures

system (energy reference: bridge-hcp on bulk Au)	$\Delta E \; (\text{meV})$
bridge-hcp on bulk Au	0
bridge-fcc on bulk Au	-8.1
bridge-hcp on relaxed Au	-316.9^{a}
bridge-fcc on relaxed Au	-343.0

^aThe -316.9 meV is the energy gained by relaxation of the Au substrate.

difference between the two sides of the bridge site is inherent to the bridge-site bonding because the substrate is unrelaxed. The energy of the system strongly depends on the orientation of the S–C bond, even for high-symmetry 3-fold hollow sites. The energy difference between the two S–C bond orientations exactly at the bridge site is 11.1 meV, which is about three times less than the energy differences at the fcc 3-fold hollow site (35.3 meV) and at the hcp 3-fold hollow site (33.0 meV). The observed energy difference for adsorption exactly on the bridge site demonstrates that the subsurface layers influence the electronic structure at the surface.

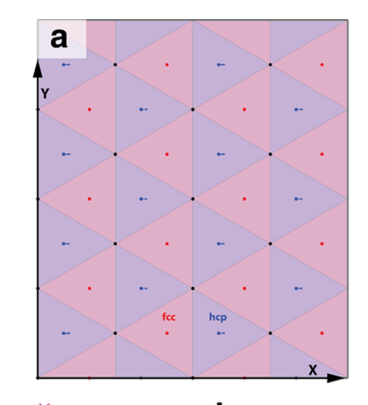
The relaxation of the bare Au(111) surface is examined first as a reference point. The top two layers are allowed to relax. We examine the displacement of each atom from its unrelaxed position and the average displacement of each layer. The latter is calculated by averaging the displacement of the 16 Au atoms in each layer. For discussion, we separate the motion of the Au atoms into two components, in the plane of the substrate (inplane: xy-plane) and perpendicular to the plane of the substrate (out-of-plane: along the z axis). As shown in Figure 1, the +x direction in the simulation coordinates is along the $[11\overline{2}]$ crystallographic direction, the +y is along the $[\overline{1}10]$, and the +z is along the [111], the surface normal. The average displacement of the Au layers is given in Table 2. The displacement of the individual atoms is shown in Figure 3 and magnified $10\times$ for visualization.

Relaxation of the bare Au substrate results in significant outof-plane relaxation as expected (Table 2). The slab expands in the [111] direction pushing the top Au layer into the vacuum (0.0571 Å), while the second layer moves closer to the third layer (0.0058 Å) (Figure 3b). This expansion is caused by the formation of a surface dipole due to the work function of the Au and the truncation of the lattice. The average in-plane

Table 2. Displacement (Å) for the Top Two Au Layers from Their Unrelaxed Positions by Simulation a

system (coordinate				
reference: unrelaxed Au)	layer	\overline{x} (Å)	\overline{y} (Å)	\overline{z} (Å)
relaxed bare Au	top layer	0.0002	0	0.0571
	second layer	0.0202	0.0001	-0.0058
bridge-fcc on relaxed Au	top layer	0.0608	0	0.0718
	second layer	-0.0045	0	0.0011
bridge-hcp on relaxed Au	top layer	0.0326	0.0072	0.0715
	second layer	-0.0064	0.0017	0.0013

"The net displacement is considered to be zero if it is less than 10^{-4} Å. While we report these numbers, we do not believe that the DFT is accurate to four decimal places. Nevertheless, they have a comparative value.



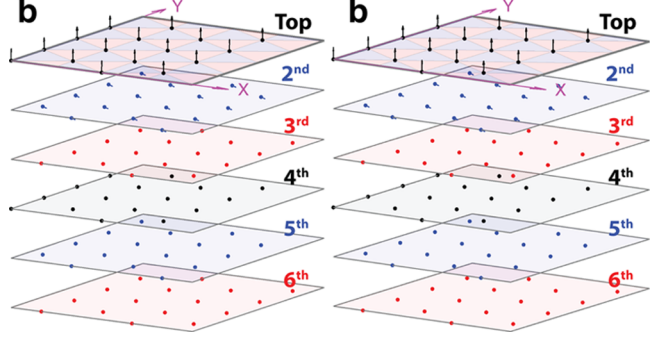


Figure 3. Au(111) surface after relaxation showing the displacement vectors. (a) Top-down view showing the top three Au layers. The top layer atoms (black) are at the vertices of the 3-fold hollow site triangles. The second layer atoms (blue) are below the hcp 3-fold hollow sites (blue triangles), and the third layer atoms (red) are below the fcc 3-fold hollow sites (red triangles). (b) Parallel-view stereo pair of the side view of the relaxed Au substrate. Arrows represent the deviation of the Au atoms compared to their ideal unrelaxed position. The arrow length is magnified 10× for visualization. The atoms are shown in their initial unrelaxed position with the displacement vectors originating from their unrelaxed positions.

displacement is more than two orders of magnitude smaller than the average out-of-plane motion of the top Au layer. In contrast, the second layer shifts in-plane (0.0202 Å) along the $+\alpha$ axis, which we believe to be a simulation artifact. Note that although in nature, the Au(111) surface undergoes the well-known herringbone reconstruction, it is not our intent to simulate that because the reconstruction is lifted by alkanethiol adsorption. ²³ Furthermore, simulating the herringbone recon-

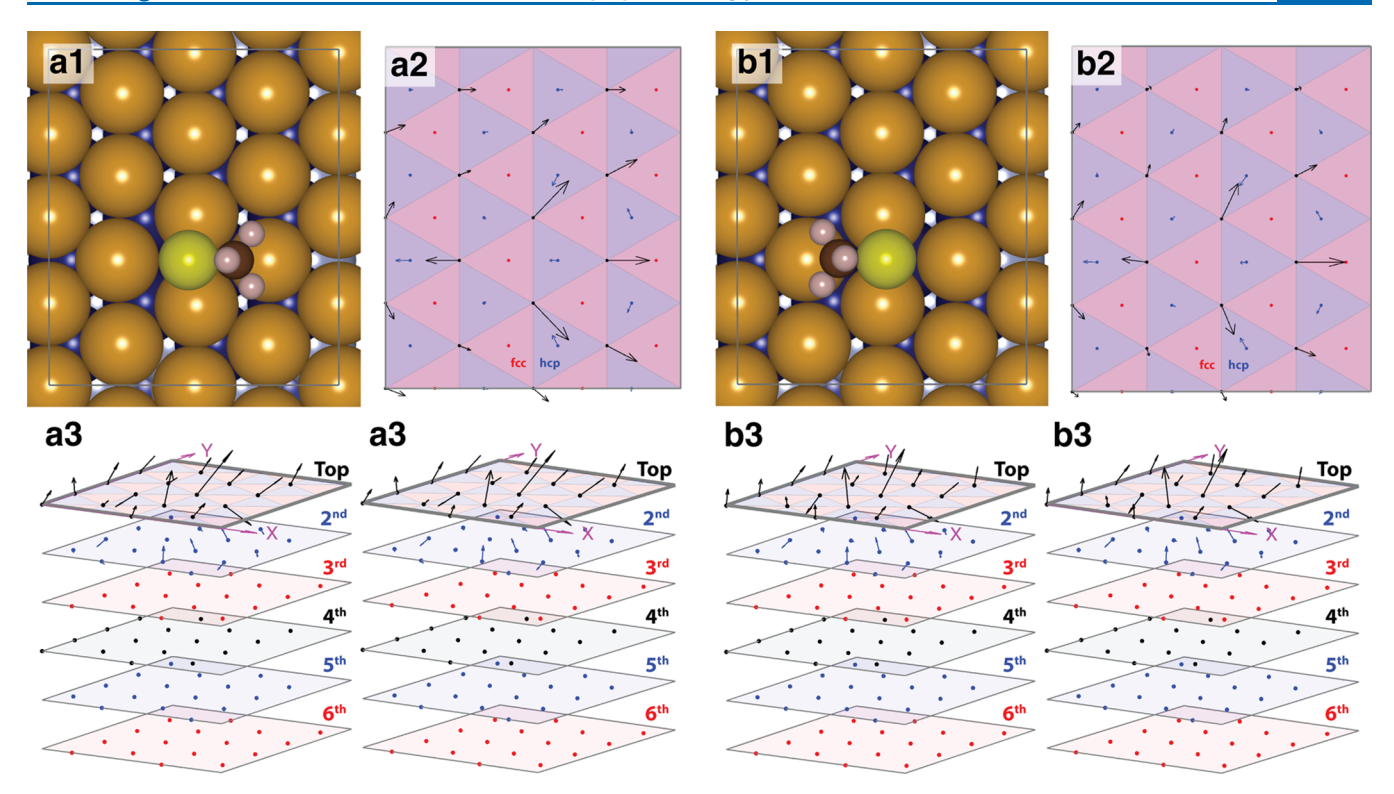


Figure 4. Au atom displacement for SCH_3 adsorbed at (a) bridge-fcc and (b) bridge-hcp sites. (a1, b1) Top-down view showing the atomic position for the adsorbates on the surface. (a2, a3, b2, b3) Views showing the displacement of the Au atoms due to relaxation. The arrows are magnified $10\times$ for visualization (see Figure 3 for a detailed description). (a2, b2) Top-down views showing the top three Au layers and their inplane displacement vectors. (a3, b3) Parallel-view stereo pairs showing all the layers with their relaxation vectors in 3D.

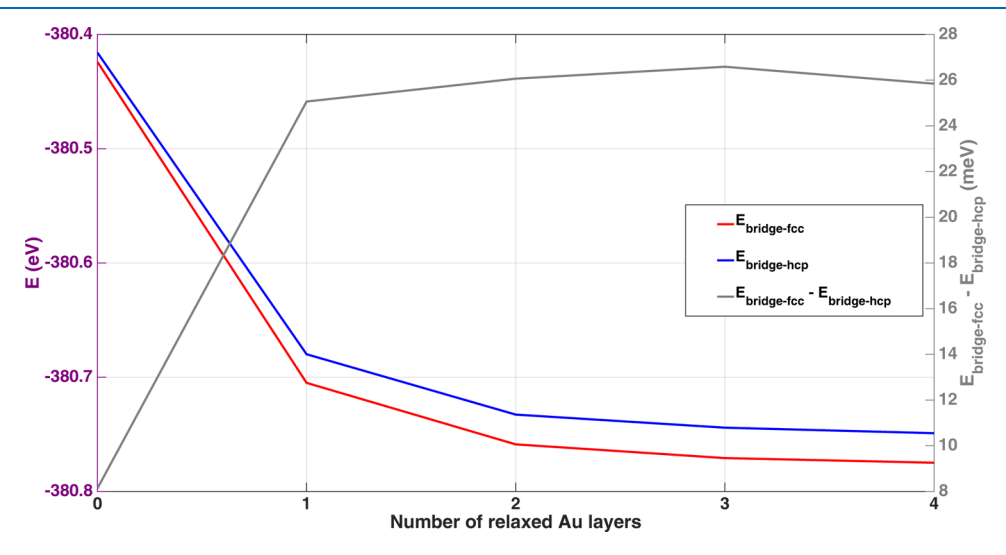


Figure 5. Effect of the number of relaxed Au layers on the bridge-fcc and bridge-hcp system energies. Dependence of the system energy (E) on the number of relaxed Au layers is shown for the bridge-fcc and bridge-hcp sites (left axis). The energy difference between bridge-hcp and bridge-fcc sites is essentially independent on the number of Au layers allowed to relax (within 1 meV) (right axis).

struction requires a larger $(22 \times \sqrt{3})$ unit cell containing extra surface atoms (46 surface Au atoms in 44 bulk positions).²⁴

Next, we turn our attention to the Au relaxation in the presence of bridge-adsorbed SCH₃. The SCH₃ is initially adsorbed at the bridge site with the S–C bond either hcp- or fcc-oriented. These initial structures relaxed to the bridge-fcc (Figure 4a) or bridge-hcp sites (Figure 4b), respectively. All simulations are started with the Au in the unrelaxed positions similar to the bare Au relaxation with the top two Au layers allowed to relax. The energy difference between the bridge-fcc

and bridge-hcp sites increases to 26.1 meV, consistent with previous calculations (Table 1, difference between the last two lines). The average out-of-plane displacement of the top two Au layers is qualitatively similar to the bare Au. The top layer expands about 25% more, while the second layer moved far less in magnitude but in the opposite direction compared to the bare Au, consistent with changes to the work function on adsorption (Table 2). The average in-plane displacements of the first Au layer occur almost exclusively in the +x direction for both adsorption sites, an indication of the asymmetry

induced by the adsorption of SCH₃. The bridge-site Au atoms are displaced away from the fcc 3-fold hollow site, although the sulfur atom moves in the opposite directions for bridge-fcc and bridge-hcp sites. The relaxation for the second layer is an order of magnitude smaller in the opposite direction. We expect that the bridge-site mirror plane symmetry should also be manifested in the Au relaxation. This symmetry is well preserved for the bridge-fcc site where the average displacement in y is zero (within the floating-point accuracy). In contrast, the bridge-hcp site shows a small asymmetry in y. To test if this was a convergence problem, we modified the resultant structure by enforcing the mirror plane symmetry. The simulation was run again using this symmetric initial condition that was now very close to the energy-minimized structure (see Figure S5 and related discussion). This procedure reproduced the original y asymmetry. The nonzero average y component for the bridge-hcp is a property of this configuration but may be an artifact of another aspect of the simulation.

We explored the effect of relaxing a different number of Au(111) layers (0-4) on the system energy and energy difference between the bridge-fcc and bridge-hcp adsorption sites. This is an important consideration because the substrate relaxation enhances the energy difference between the two sites. The results of this study are shown in Figure 5. The largest change in system energy occurs with relaxation of the first layer and continues to decrease monotonically. Relaxing more than four layers would require adding more layers to our six-layer slab model. Surprisingly, the energy difference is not very sensitive to the number of layers relaxed. Compared to the two-layer relaxed system already discussed, the energy difference is 1.0 meV smaller for one layer relaxed and 0.5 and 0.2 meV larger for three and four layers relaxed. The displacements of the atoms in each layer with three and four layers relaxed are not remarkably different from only two layers relaxed (Figure S3). We conclude that relaxing the top two layers is adequate for this study.

The van der Waals interactions of the methyl group and the Au surface could introduce an asymmetry between the two sites. In both sites, one of the methyl hydrogens is oriented away from the surface in these energy-minimized structures. Therefore, we would expect the van der Waals interactions to be very similar. We can eliminate this steric effect as the origin of the asymmetry by replacing the methyl group with hydrogen. The energy and structural asymmetry persisted between the hcp- and fcc-oriented SH. The S atom position and Au relaxation were large, as described above. Details of these calculations can be found in the Supporting Information. We conclude that the observed geometry is a characteristic of the S atom bonding at the bridge site; the asymmetry is due to the Au surface and not an artifact of nonbonding interaction of the methyl group with the Au surface.

We turn now to the bonding geometry of the S atom. In all cases, Au atoms of the bridge bond relax to increase the angle between the two Au-S bonds, which brings the S atom closer to the surface (Table 3). From another perspective, the S atom bonds to the surface in a manner that forces the bridge-bonded Au atoms to move apart. Figure 4 shows the displacement of the individual Au atoms. The height of the S atom is the furthest away from the top layer (S atom to the average zcoordinate of the top layer Au atoms) for the bridge-hcp and closest for the bridge-fcc. The height difference is 0.0443 Å between bridge-hcp and bridge-fcc, showing that the S atom

Table 3. Geometric Parameters of the SCH₃ Adsorbate^a

	bridge-fcc on relaxed	bridge-hcp on relaxed
parameter	Au	Au
Purumeter	114	110
S-top layer (Å)	1.99 [2.06]	2.03 [2.07]
$S-Au_1$ (Å)	2.44 [2.52]	2.45 [2.52]
S-Au ₂ (Å)	2.44 [2.52]	2.45 [2.54]
Au_1-Au_2 (Å)	3.14 [2.89]	3.10 [2.89]
Au_2 -S- Au_1 (°)	79.83 [69.77]	78.54 [69.57]
S-C and surface normal	59.44 [59.76]	58.71 [60.25]
()		
Au_1 -S-C (°)	106.84 [110.08]	108.05 [108.72]
Au_2 -S-C (°)	106.84 [110.08]	108.76 [109.91]

^aThe values in the square brackets are for the relaxed SCH₃ on unrelaxed Au.

moves closer to the surface for bridge-fcc due to stronger adsorption. The bond distances between the S atom and the bridging Au atoms (S-Au₁ and S-Au₂, Figure 1) are symmetric for both the bridge-fcc and bridge-hcp. The bond angle between the bridging atoms and the S atom (Au₂-S-Au₁) is within 1° for all cases studied. The Au-S-C bond angles for the methanethiol adsorption are within 106-109°, in agreement with previous results. 16

The preference of the S–C bond azimuthal orientations, hcp for bridge-fcc and fcc for bridge-hcp, can be understood in terms of a simple qualitative chemical picture. By considering the S atom bonding orbitals as approximately sp³ hybridized, the S bonds prefer to be oriented in approximately tetrahedral geometries (tetrahedral, pyramidal, and bent). At the bridge site, the S atom is in a 3-coordinate pyramidal bonding geometry, with one bond to each of the bridging atoms and the third to the methyl. The S-C bond is at an angle to the surface normal such that the Au-S-C bond angles are approximately the tetrahedral angle. Only the fcc and hcp orientations satisfy the pyramidal bonding geometry. This picture is also consistent with results for the energy-minimized structures of SCH₃ adsorbed at 3-fold hollow²⁵ and atop sites.¹⁸ In the former, the S atom is four-coordinate (tetrahedral), with one bond to each of the three surface Au atoms and the S-C bond normal to the surface. In the latter, the S atom is twocoordinate (bent) with the Au–S–C bond angle again close to the tetrahedral angle. The Au-S-Au bond angles observed are smaller than the tetrahedral angle but are expected to have significant d contribution. This qualitative picture gives useful insight into the bonding geometry on Au(111).

Our results demonstrate that the inherent asymmetry of the bridge-fcc and bridge-hcp is amplified by the relaxation of the substrate as demonstrated by the increased difference in adsorption energy and the asymmetric relaxation of the Au surface. We also demonstrate that the energy of an adsorption site depends on the S-C bond azimuth with respect to the underlying substrate. The strength of the energy dependence varies from site to site.

CONCLUSIONS

In our study, we have chosen the simplest methanethiol adsorption scenario on the Au(111) substrate without adatoms and/or vacancies to study the asymmetry of the bridge-fcc and bridge-hcp sites and the effect of the substrate relaxation on the asymmetry. The energy of an adsorption site depends on the orientation of the S-C bond. The line scan from the fcc 3-fold hollow site through the bridge site to the hcp 3-fold hollow site

Table 4. Comparison of the Optimized Au Lattice Constant (Å) for Different DFT Functionals

PAW+LDA +D2	USPP+LDA +D2	PAW +LDA	USPP +LDA	experiment	PAW+PBE +D2	PAW+GGA +D2	USPP+GGA +D2	PAW +PBE	PAW +GGA	USPP +GGA
4.01	4.02	4.05	4.07	4.08	4.10	4.12	4.13	4.16	4.18	4.18

shows the inherent bridge-site asymmetry and its dependence on the S-C bond orientation. Then, the bridge-adsorbed SCH₃ is allowed to relax to its energy-minimized structure, and the S atom moves to the side of the bridge opposite to the methyl group (bridge-fcc and bridge-hcp sites). When the Au surface is also allowed to relax, the SCH₃ exhibits the same preference for different sides of the bridge, while in both cases, the bridging Au atoms are displaced away from the fcc 3-fold hollow site. The intrinsic energy difference between the bridgefcc and bridge-hcp sites on the unrelaxed bulk Au substrate is 8.1 meV due to the bridge-site bonding. The energy difference between these two sites is increased to 26.1 meV after the substrate relaxation. The relaxation of the substrate magnifies the intrinsic asymmetry of the bridge-fcc and bridge-hcp sites. The bridging Au atoms are pushed apart during the relaxation by the S atom as the Au-S-Au angle opens up, allowing the S atom to nestle closer to the surface for the bridge-fcc than the bridge-hcp. This asymmetry between these two sites is also evident on the S bond angles and the height of the S atom from the substrate. We also proposed a qualitative model for understanding the S atom bonding geometries and the S-C bond orientation.

■ THEORETICAL METHODS

Our DFT calculations are performed using the Vienna ab initio simulation package VASP 5.4.4. 26,27 These calculations are carried out with the Agave system at Arizona State's Research Computing Center. The projector augmented wave (PAW) method density functional is used for the electron-ion interaction along with the Perdew-Burke-Ernzerhof (PBE) exchange functional. 28,29 The functional is denoted as PAW-PBE, and it is most commonly used to model the adsorption of organic molecules on metal surfaces. 30-32 The van der Waals (vdW) forces play an important role in such weakly interacting systems.³³ Therefore, the dispersion correction of Grimme (DFT-D2) is included for more realistic simulation of the interaction between the adsorbate and the Au(111) substrate.³⁴ A plane wave cutoff of 300 eV is used. We also tested a higher plane wave cutoff of 400 eV. The higher cutoff resulted in only a 1 meV increase in the energy difference between the bridge-fcc site and the bridge-hcp site on the relaxed substrate, from 26.1 to 27.1 meV. The improvement is on the order of the precision of the calculation and is significantly less than the energy difference between the two structures. The Brillouin zone integration is performed using the Monkhorst-Pack sampling with $9 \times 9 \times 1$ Γ -centered k-grid for a surface unit cell. Geometries are considered optimized when the Hellmann-Feynman forces on ions are less than 10⁻² eV $Å^{-1}$. In our fully relaxed structures, the adsorbate atoms are allowed to relax in all directions during the geometry optimization. The top two layers of Au atoms are allowed to relax in our study of substrate relaxation.³⁵ For the line scan series, we control the azimuthal direction for the S-C bond as the S atom is moved in steps across the unrelaxed Au substrate using selective constraints on the absorbate. The S atom is constrained in the xy-plane and allowed to relax in z alone to maintain a specified position on the substrate. The C atom is

constrained in *y* and allowed to relax in the *xz*-plane. The H atoms are unconstrained. In this way, the Au–S–CH₃ bond lengths and angles are allowed to relax while the azimuthal orientation of the S–C bond is constrained.

Selecting a set of DFT parameters that closely replicate the Au lattice constant is a natural starting point. An accurate representation of the Au(111) substrate is important to achieve the proper adsorbate interactions. The weighted average of the Au lattice constant of 4.07895(4) Å (25 °C) is experimentally known to much higher accuracy than current DFT results typically yield. 36,37 The simulated lattice constant depends on the combination of the pseudo-potential, the exchange-correlation functional, and the dispersion correction. 30,38,39 Without the dispersion correction, DFT has reported lattice constants as high as 4.18 Å (~2.5% higher than the experimental value), which results in ~7.6% lower electron density. 40 To put this large lattice constant into perspective, to achieve this through thermal expansion requires a temperature of 1670 K, well above the melting point of gold (Figure S1).41 Inclusion of the dispersion correction significantly improved the lattice constant (4.094 Å) along with other properties of the Au lattice.⁴²

To determine suitable DFT functionals for our study, we explored combinations of two pseudo-potentials (PAW and ultrasoft pseudo-potential (USPP)), three exchange functionals (PBE, generalized gradient approximation (GGA), and local density approximation (LDA)), and the D2 correction to determine which produces a lattice constant closest to the experimental value. Following the conventional equation of state approach, single-point energy bulk calculations were performed while varying the unit cell dimensions. The energy versus lattice constant values were fit to a fifth order polynomial (Figure S2). The vertex of the resulting curve yields a minimum energy lattice constant for that functional (Table 4). The combination of PAW, PBE, and the D2 dispersion correction yields a lattice constant of 4.10 Å, which is second closest to the experimental value after USPP+LDA. Although the latter combination achieves a closer lattice constant, the LDA functional lacks the accurate representation of more localized and fast varying electron densities in atoms and clusters. 43 Therefore, we chose the PAW+PBE combination with the D3 dispersion for our study.

The most common recipe for DFT surface studies is to construct a supercell composed of a substrate slab and a vacuum layer. The vacuum layer must be thick enough that the interaction between the periodic images can be neglected (viz. the top of the slab and its adsorbates with the periodic image of the bottom of the slab on the other side of the vacuum layer). However, increasing the volume of the supercell is computationally expensive in the plane wave basis, so the vacuum thickness is limited in practice. A vacuum thickness of 10–15 Å has been found to be a good compromise. ^{20,44} The periodic images of the slab in our simulations are separated by 13 Å of vacuum.

The number of Au layers in the slab needs to be large enough to reduce the interaction between the top and the bottom of the slab. Increasing the number of Au layers adds computational expense. There are also symmetry considerations; the fcc structure of the Au lattice has a three-layer ABC stacking along the [111] direction (Figure 1).⁴⁵ Four layers of Au are adequate to approximate the bulk gold substrate, but for a clean termination of the bulk Au(111), we include six layers to preserve the ABC stacking.^{20,44,46}

We have chosen a $(4 \times 2\sqrt{3})$ rectangular unit cell with 16 Au atoms per layer to provide lateral separation between the adsorbate images and simulate a low adsorption surface density. To minimize the effect of the interand intrachain vdW interaction of the adsorbates on the system energy, we have used the shortest alkane chain length (methanethiol, SCH₃).

Placing an adsorbate on one side of the slab results in an asymmetric charge density with respect to the top and bottom surfaces of the slab. In addition, allowing only the atoms on one side of the slab to relax introduces an analogous asymmetry. Both create a difference in the electrostatic potential at the cell boundary, which produces an artificial electric field in the vacuum region. To compensate, a tunable dipole layer is introduced in the vacuum region of the supercell, which self-consistently compensates for the electrostatic potential difference and nulls the electric field. 47,48

ASSOCIATED CONTENT

5 Supporting Information

The Supporting Information is available free of charge at https://pubs.acs.org/doi/10.1021/acsomega.0c02328.

Temperature dependence and extrapolation of the Au lattice constant; equation of state calculations for Au; Au atomic displacement with SCH₃ adsorbed for one, two, three, and four Au(111) layers relaxed; relaxation of the Au(111) surface with adsorbed SH in two orientations; and testing the deviation from bridge-site mirror plane symmetry of the bridge-hcp site Au surface relaxation (PDF)

Atomic coordinate files for the DFT computations (ZIP)

AUTHOR INFORMATION

Corresponding Author

Lloyd A. Bumm — Homer L. Dodge Department of Physics and Astronomy, University of Oklahoma, Norman, Oklahoma 73019, United States; orcid.org/0000-0003-2301-8193; Email: bumm@ou.edu

Authors

Soumya Bhattacharya — Homer L. Dodge Department of Physics and Astronomy, University of Oklahoma, Norman, Oklahoma 73019, United States; Occid.org/0000-0001-8544-3174

Gil Speyer – Research Computing, Arizona State University, Tempe, Arizona 85287, United States

David K. Ferry — School of Electrical, Computer and Energy Engineering, Arizona State University, Tempe, Arizona 85287, United States

Complete contact information is available at: https://pubs.acs.org/10.1021/acsomega.0c02328

Author Contributions

All authors contributed equally.

Notes

The authors declare no competing financial interest.

ACKNOWLEDGMENTS

We acknowledge support from NSF CHE-1710102. Allocation time for DFT simulations was performed using the Agave system at Arizona State's Research Computing Center and the OU Supercomputing Center for Education & Research (OSCER) at the University of Oklahoma (OU). S.B. acknowledges the Carl. T. Bush Fellowship and Homer L. Dodge Fellowship for support. We gratefully acknowledge the support of NVIDIA Corporation with the donation of the Tesla K40 GPU used for this research. Authors also wish to thank M. Yothers for helpful discussion.

REFERENCES

- (1) Nuzzo, R. G.; Allara, D. L. Adsorption of Bifunctional Organic Disulfides on Gold Surfaces. *J. Am. Chem. Soc.* **1983**, *105*, 4481–4483.
- (2) Bain, C. D.; Biebuyck, H. A.; Whitesides, G. M. Comparison of self-assembled monolayers on gold: coadsorption of thiols and disulfides. *Langmuir* 1989, 5, 723–727.
- (3) Casalini, S.; Bortolotti, C. A.; Leonardi, F.; Biscarini, F. Self-Assembled Monolayers in Organic Electronics. *Chem. Soc. Rev.* **2017**, 46, 40–71.
- (4) Magnussen, O. M.; Vogt, M. R.; Scherer, J.; Behm, R. J. Double-Layer Structure, Corrosion and Corrosion Inhibition of Copper in Aqueous Solution. *Appl. Phys. A: Mater. Sci. Process.* **1998**, *66*, S447—S451.
- (5) Love, J. C.; Estroff, L. A.; Kriebel, J. K.; Nuzzo, R. G.; Whitesides, G. M. Self-Assembled Monolayers of Thiolates on Metals as a Form of Nanotechnology. *Chem. Rev.* **2005**, *105*, 1103–1170.
- (6) Fujihira, M.; Tani, Y.; Furugori, M.; Akiba, U.; Okabe, Y. Chemical Force Microscopy of Self-Assembled Monolayers on Sputtered Gold Films Patterned by Phase Separation. *Ultramicroscopy* **2001**, *86*, 63–73.
- (7) Ulman, A. Formation and Structure of Self-Assembled Monolayers. Chem. Rev. 1996, 96, 1533–1554.
- (8) Vericat, C.; Vela, M. E.; Benitez, G.; Carro, P.; Salvarezza, R. C. Self-Assembled Monolayers of Thiols and Dithiols on Gold: New Challenges for a Well-Known System. *Chem. Soc. Rev.* **2010**, 39, 1805–1834.
- (9) Reimers, J. R.; Ford, M. J.; Marcuccio, S. M.; Ulstrup, J.; Hush, N. S. Competition of van der Waals and Chemical Forces on Gold–Sulfur Surfaces and Nanoparticles. *Nat. Rev. Chem.* **2017**, *1*, No. 0017.
- (10) Camillone, N., III; Chidsey, C. E. D.; Liu, G.-Y.; Scoles, G. Superlattice Structure at the Surface of a Monolayer of Octadecanethiol Self-Assembled on Au(111). *J. Chem. Phys.* **1993**, *98*, 3503–3511.
- (11) Delamarche, E.; Michel, B.; Gerber, C.; Anselmetti, D.; Guentherodt, H.-J.; Wolf, H.; Ringsdorf, H. Real-Space Observation of Nanoscale Molecular Domains in Self-Assembled Monolayers. *Langmuir* **1994**, *10*, 2869–2871.
- (12) Poirier, G. E.; Tarlov, M. J. The c(4×2) Superlattice of *n*-Alkanethiol Monolayers Self-Assembled on Au(111). *Langmuir* **1994**, 10, 2853–2856.
- (13) Lüssem, B.; Müller-Meskamp, L.; Karthäuser, S.; Waser, R. A New Phase of the $c(4 \times 2)$ Superstructure of Alkanethiols Grown by Vapor Phase Deposition on Gold. *Langmuir* **2005**, *21*, 5256–5258.
- (14) Grönbeck, H.; Häkkinen, H.; Whetten, R. L. Gold-Thiolate Complexes form a Unique c(4×2) Structure on Au(111). *J. Phys. Chem. C* **2008**, *112*, 15940–15942.
- (15) Torrelles, X.; Pensa, E.; Cortés, E.; Salvarezza, R.; Carro, P.; Hernández Guerrero, C.; Ocal, C.; Barrena, E.; Ferrer, S. Solving the Long-Standing Controversy of Long-Chain Alkanethiols Surface Structure on Au(111). *J. Phys. Chem. C* **2018**, *122*, 3893–3902.

- (16) Yourdshahyan, Y.; Rappe, A. M. Structure and Energetics of Alkanethiol Adsorption on the Au(111) Surface. *J. Chem. Phys.* **2002**, 117, 825–833.
- (17) Cao, Y.; Ge, Q.; Dyer, D. J.; Wang, L. Steric Effects on the Adsorption of Alkylthiolate Self-Assembled Monolayers on Au (111). *J. Phys. Chem. B* **2003**, *107*, 3803–3807.
- (18) Nagoya, A.; Morikawa, Y. Adsorption States of Methylthiolate on the Au(111) Surface. *J. Phys.: Condens. Matter* **2007**, *19*, 365245.
- (19) Maksymovych, P.; Sorescu, D. C.; Yates, J. T., Jr. Gold-Adatom-Mediated Bonding in Self-Assembled Short-Chain Alkanethiolate Species on the Au(111) Surface. *Phys. Rev. Lett.* **2006**, *97*, 146103–146104.
- (20) Cossaro, A.; Mazzarello, R.; Rousseau, R.; Casalis, L.; Verdini, A.; Kohlmeyer, A.; Floreano, L.; Scandolo, S.; Morgante, A.; Klein, M. L.; Scoles, G. X-ray Diffraction and Computation Yield the Structure of Alkanethiols on Gold(111). *Science* **2008**, 321, 943–946.
- (21) Bhattacharya, S.; Yothers, M. P.; Huang, L.; Bumm, L. A. Interaction of the $(2\sqrt{3}\times3)$ rect. Adsorption-Site Basis and Alkyl-Chain Close Packing in Alkanethiol Self-Assembled Monolayers on Au(111): A Molecular Dynamics Study of Alkyl-Chain Conformation. ACS Omega 2020, 5, 13802–13812.
- (22) Reimers, J. R.; Ford, M. J.; Halder, A.; Ulstrup, J.; Hush, N. S. Gold surfaces and nanoparticles are protected by Au(0)—thiyl species and are destroyed when Au (I)—thiolates form. *Proc. Natl. Acad. Sci. U. S. A.* **2016**, *113*, E1424—E1433.
- (23) Poirier, G. E.; Pylant, E. D. The Self-Assembly Mechanism of Alkanethiols on Au(111). Science 1996, 272, 1145–1148.
- (24) Hanke, F.; Björk, J. Structure and Local Reactivity of the Au(111) Surface Reconstruction. *Phys. Rev. B* **2013**, *87*, 235422.
- (25) Cometto, F. P.; Paredes-Olivera, P.; Macagno, V. A.; Patrito, E. M. Density Functional Theory Study of the Adsorption of Alkanethiols on Cu(111), Ag(111), and Au(111) in the Low and High Coverage Regimes. *J. Phys. Chem. B* **2005**, *109*, 21737–21748.
- (26) Kresse, G.; Furthmüller, J. Efficiency of ab-initio Total Energy Calculations for Metals and Semiconductors Using a Plane-wave Basis Set. *Comput. Mater. Sci.* **1996**, *6*, 15–50.
- (27) Kresse, G.; Joubert, D. From Ultrasoft Pseudopotentials to the Projector Augmented-wave Method. *Phys. Rev. B* **1999**, *59*, 1758–1775.
- (28) Blöchl, P. E. Projector Augmented-wave Method. *Phys. Rev. B* **1994**, *50*, 17953–17979.
- (29) Perdew, J. P.; Burke, K.; Ernzerhof, M. Generalized Gradient Approximation Made Simple. *Phys. Rev. Lett.* **1996**, *77*, 3865–3868.
- (30) Gautier, S.; Steinmann, S. N.; Michel, C.; Fleurat-Lessard, P.; Sautet, P. Molecular Adsorption at Pt(111). How Accurate are DFT Functionals? *Phys. Chem. Chem. Phys.* **2015**, *17*, 28921–28930.
- (31) Mete, E.; Yortanli, M.; Danişman, M. F. A van der Waals DFT Study of Chain Length Dependence of Alkanethiol Adsorption on Au(111): Physisorption vs. Chemisorption. *Phys. Chem. Chem. Phys.* **2017**, *19*, 13756–13766.
- (32) Yuan, D.; Liao, H.; Hu, W. Assessment of van der Waals Inclusive Density Functional Theory Methods for Adsorption and Selective Dehydrogenation of Formic Acid on Pt(111) Surface. *Phys. Chem. Chem. Phys.* **2019**, 21, 21049–21056.
- (33) Muniz-Miranda, F.; Menziani, M. C.; Pedone, A. Assessment of Exchange-Correlation Functionals in Reproducing the Structure and Optical Gap of Organic-Protected Gold Nanoclusters. *J. Phys. Chem.* C **2014**, *118*, 7532–7544.
- (34) Amft, M.; Lebègue, S.; Eriksson, O.; Skorodumova, N. V. Adsorption of Cu, Ag, and Au atoms on graphene including van der Waals interactions. *J. Phys.: Condens. Matter* **2011**, 23, 395001.
- (35) Mom, R. V.; Melissen, S. T. A. G.; Sautet, P.; Frenken, J. W. M.; Steinmann, S. N.; Groot, I. M. N. The Pressure Gap for Thiols: Methanethiol Self-Assembly on Au(111) from Vacuum to 1 bar. *J. Phys. Chem. C* **2019**, *123*, 12382–12389.
- (36) Eisenmann, B.; Schäfer, H. Structure data of elements and intermetallic phases. In *Landolt-Börnstein. Group III, Condensed Matter*; Hellwege, K.-H.; Hellwege, A. M., Eds. Springer: Berlin, 2006; Vol. 14a.

- (37) Wyckoff, R. W. G. Crystal Structures; 2nd ed.; John Wiley & Sons: New York, 1965, Vol. 1.
- (38) Lee, K.; Murray, É. D.; Kong, L.; Lundqvist, B. I.; Langreth, D. C. Higher-Accuracy van der Waals Density Functional. *Phys. Rev. B* **2010**, 82, No. 081101.
- (39) Steinmann, S. N.; Corminboeuf, C. Comprehensive Benchmarking of a Density-Dependent Dispersion Correction. *J. Chem. Theory Comput.* **2011**, *7*, 3567–3577.
- (40) Bilić, A.; Reimers, J. R.; Hush, N. S.; Hafner, J. Adsorption of Ammonia on the Gold (111) Surface. *J. Chem. Phys.* **2002**, *116*, 8981–8987.
- (41) Haynes, W. M.; Lide, D. R.; Bruno, T. J. CRC Handbook of Chemistry and Physics; 97th ed.; CRC Press: Boca Raton, 2016, DOI: 10.1201/9781315380476.
- (42) Seema, P.; Behler, J.; Marx, D. Force-Induced Mechanical Response of Molecule–Metal Interfaces: Molecular Nanomechanics of Propanethiolate Self-Assembled Monolayers on Au(111). *Phys. Chem. Chem. Phys.* **2013**, *15*, 16001–16011.
- (43) Rietmann, T.; Sohn, S.; Schröder, M.; Lipinsky, D.; Arlinghaus, H. F. Comparison of Detection Efficiencies of Negatively Charged Gold-Alkanethiolate-, Gold-Sulfur- and Gold-Clusters in ToF-SIMS. *Appl. Surf. Sci.* **2006**, 252, 6640–6643.
- (44) Wang, J.-G.; Selloni, A. The c(4×2) Structure of Short- and Intermediate-Chain Length Alkanethiolate Monolayers on Au(111): A DFT Study. *J. Phys. Chem. C* **2007**, *111*, 12149–12151.
- (45) Jette, E. R.; Foote, F. Precision Determination of Lattice Constants. J. Chem. Phys. 1935, 3, 605–616.
- (46) Grönbeck, H.; Häkkinen, H. Polymerization at the Alkylthiolate-Au(111) Interface. *J. Phys. Chem. B* **2007**, *111*, 3325–3327.
- (47) Neugebauer, J.; Scheffler, M. Adsorbate-substrate and Adsorbate-adsorbate Interactions of Na and K Adlayers on Al(111). *Phys. Rev. B* **1992**, *46*, 16067–16080.
- (48) Bengtsson, L. Dipole Correction for Surface Supercell calculations. *Phys. Rev. B* **1999**, *59*, 12301–12304.

Supporting information

A Comprehensive Study of the Bridge Site and Substrate Relaxation Asymmetry for Methanethiol Adsorption on Au(111) at Low Coverage

Soumya Bhattacharya[†], Gil Speyer[#], David K. Ferry[‡], and Lloyd A. Bumm[†]*

[†]Homer L. Dodge Department of Physics and Astronomy, University of Oklahoma, Norman, OK, 73019

*Research Computing, Arizona State University, Tempe, Arizona, 85287

[‡]School of Electrical, Computer and Energy Engineering, Arizona State University,

Tempe, Arizona, 85287

A. Temperature Dependence and Extrapolation of the Au lattice Constant

We are interested to use the temperature dependent lattice constant of Au as a point of reference for the DFT-predicted lattice constants. See the main text for the full context. The thermal expansion coefficient of the Au lattice is taken from Nix and MacNair and it is used to calculate the Au-Au distance for extrapolated temperature as shown in the Figure S1.¹ The data are presented in terms of the Au-Au nearest-neighbor distance (d) instead of the fcc lattice constant (a). The relationship is $d = a/\sqrt{2}$.

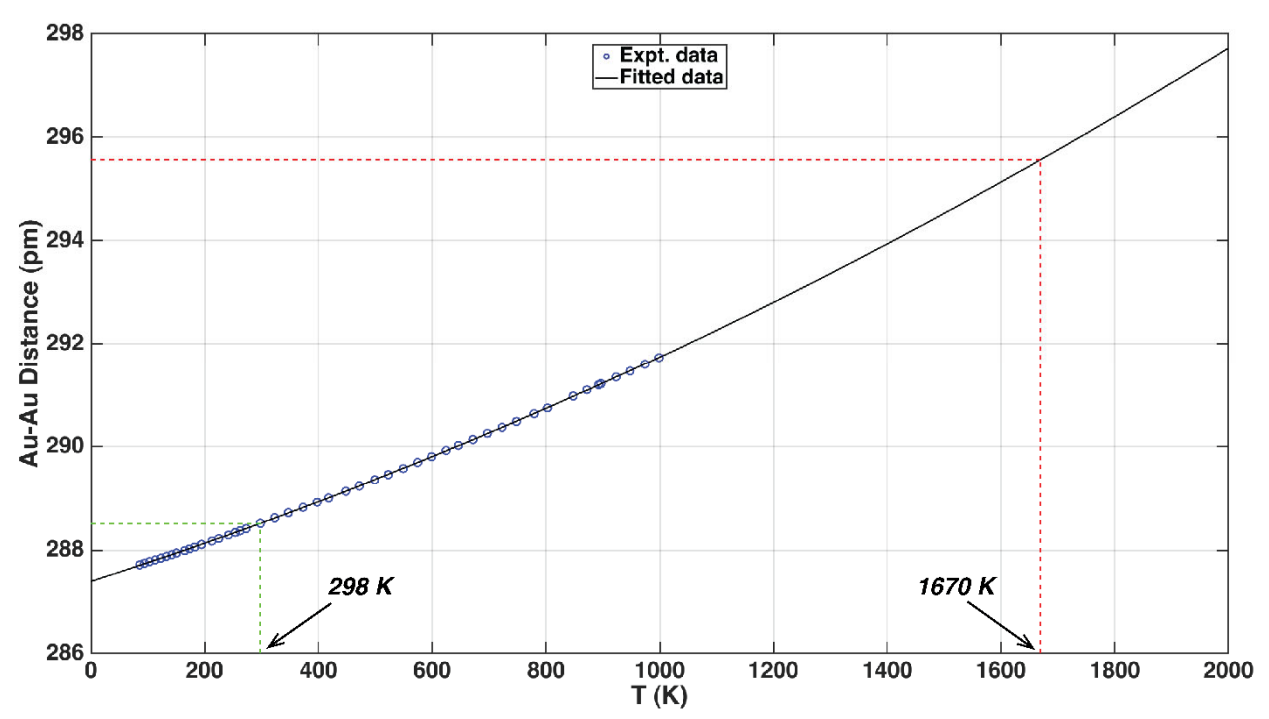


Figure S1. The thermal expansion of the Au lattice constant is shown. The Au-Au distance at room temperature (298 K) is 288.43 pm. The expanded Au-Au distance of 295.57 pm corresponds to an extrapolated temperature of 1670 K.

B. Equation of State Calculations for Au

See the main text for details. The data in Table 4 is repeated in Table S1, but is presented here in the order given in the legend of Figure S2.

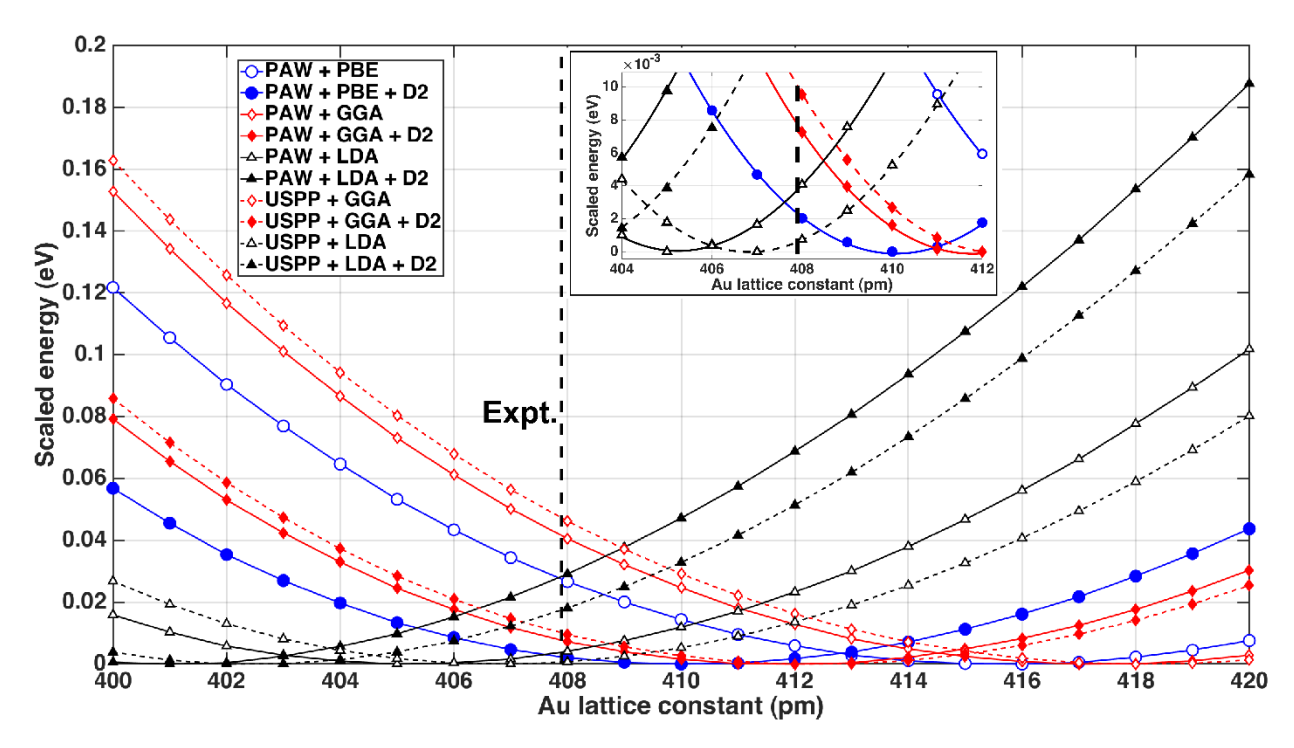


Figure S2. The equation of state calculation on the unreconstructed Au for a combination of DFT functionals. The vertical dashed line represents the experimental value of the Au lattice constant at 25 °C. The symbols are the calculated values. The lines are a 5th-order polynomial fit to those values. The inset is a view of the same data expanded to better visualize the minima close to the experimental lattice constant. The most suitable combination to replicate the experimental lattice constant is (PAW + PBE + D2).

Table S1. Comparison of the optimized Au lattice constant (Å) for different DFT functionals.

PAW+PBE	PAW+PBE+D2	PAW+GGA	PAW+GGA+D2	PAW+LDA	PAW+LDA+D2	USPP+GGA	USPP+GGA+D2	USPP+LDA	USPP+LDA+D2	Experiment
4.16	4.10	4.18	4.12	4.05	4.01	4.18	4.13	4.07	4.02	4.08

C. Au Atomic Displacement with SCH₃ Adsorbed for 1, 2, 3, and 4 Au(111) Layers Relaxed

We explored the effect of relaxing a different number of Au(111) layers (0-4) on the system energy and energy difference between the bridge-fcc and the bridge-fcc adsorption sites. See the main text for context. The displacements of the atoms in each layer are shown in Figure S3 and are not remarkable beyond the observation for two layers relaxed. We conclude that relaxing the top two layers is adequate for this study.

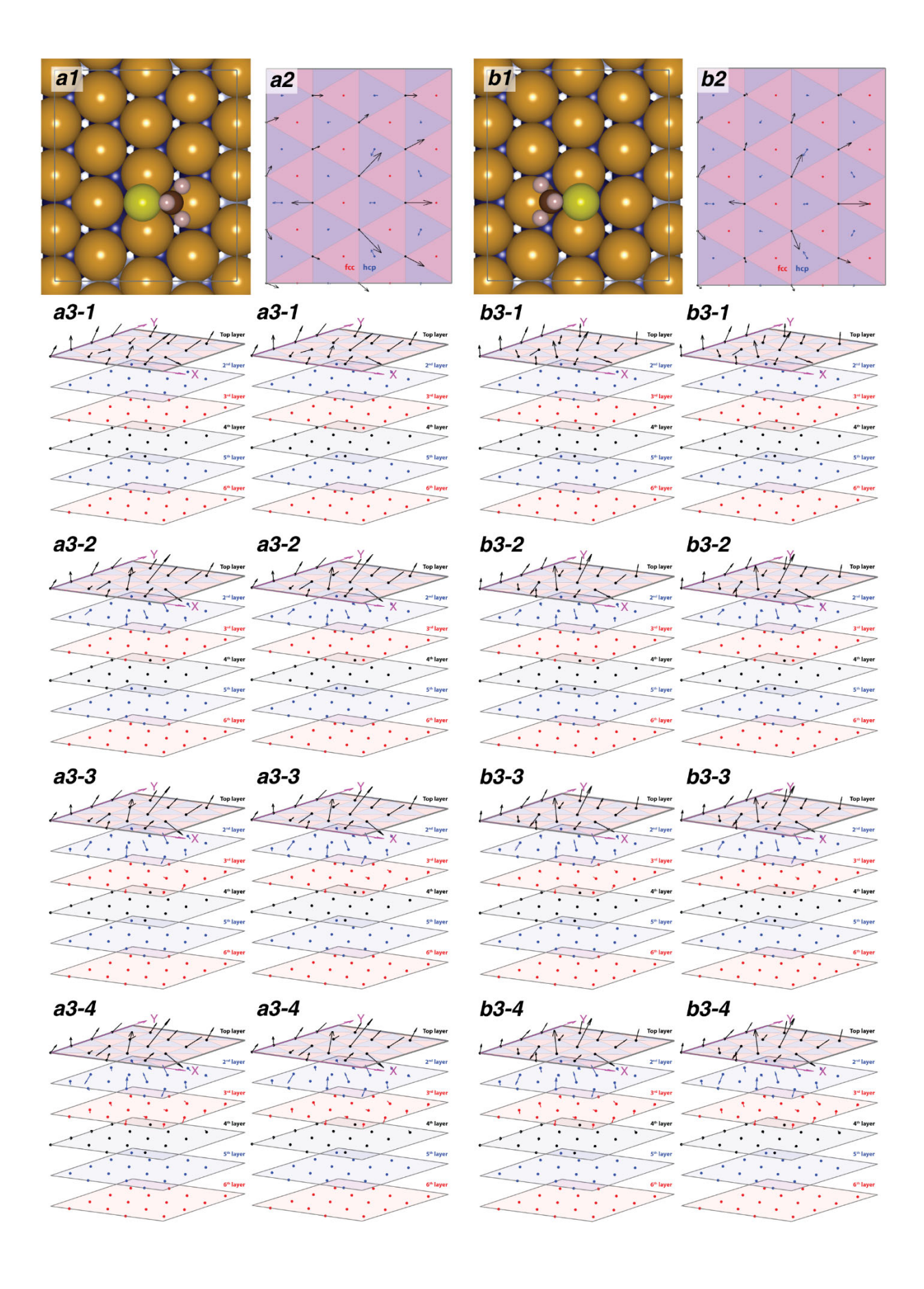


Figure S3. The Au atom displacement for SCH₃ adsorbed at the bridge-fcc (a) and the bridge-hcp (b) sites for one to four top layers relaxed. (a1 and b1) The top-down view showing the atomic position for the adsorbates on the surface. (a2 and b2) Top-down views showing the top three Au layers and their in-plane displacement vectors for the two top layers relaxed. (a3 and b3) Parallel-view stereo pairs showing all the layers with their relaxation vectors in 3D. Views showing the displacement of the Au atoms due to relaxation of only top layer (a3-1 and b3-1), top two layers (a3-2 and b3-2), top three layers (a3-3 and b3-3), and top four layers (a3-4 and b3-4). The arrows are magnified $10 \times$ for visualization (see Figure 4 for a detailed description).

D. Relaxation of the Au(111) Surface with Adsorbed SH in Two Orientations

The SH was initially absorbed at the bridge site on the unrelaxed substrate with S-C bond either hcp or fcc oriented. In one study, only the adsorbate could relax. In another, the top two layers of the Au substrate are relaxed along with the adsorbate. In both studies, the SH behaved very similar to SCH₃, where the S atom relaxed to the bridge-fcc (hcp oriented) or the bridge-hcp (fcc oriented) site dependent on the S-C bond orientation. The Au surface relaxation is shown in Figure S4, analogous to Figure 4 for SCH₃. The results of the SH study are summarized in Tables S2-S4. Table S5 compares the geometric parameters for SH and SCH₃. The sulfur atom is further away from the surface compared to the SCH₃, indicating a weaker Au-S bond for SH. The polar angle of the S-H bond with respect to the surface normal is larger than the S-C bond. The polar angle for SH is larger for the bridge-hcp adsorption than the bridge-fcc adsorption, in contrast with the SCH₃ adsorption. The sulfur atom sits closer to the surface at the bridge-fcc site compare to the bridge-hcp site, shown in Table S5. The bridging Au atoms are pushed apart less by SH than SCH₃. The Au-S-H bond angles are ~98° compared to Au-S-C which are ~108° indicating the bonding at the S atom is different. While the energy difference on the unrelaxed surface, 7.5 meV, is very similar to SCH₃, relaxation of the surface does not increase the energy asymmetry for SH but slightly decreases it to 6.2 meV.

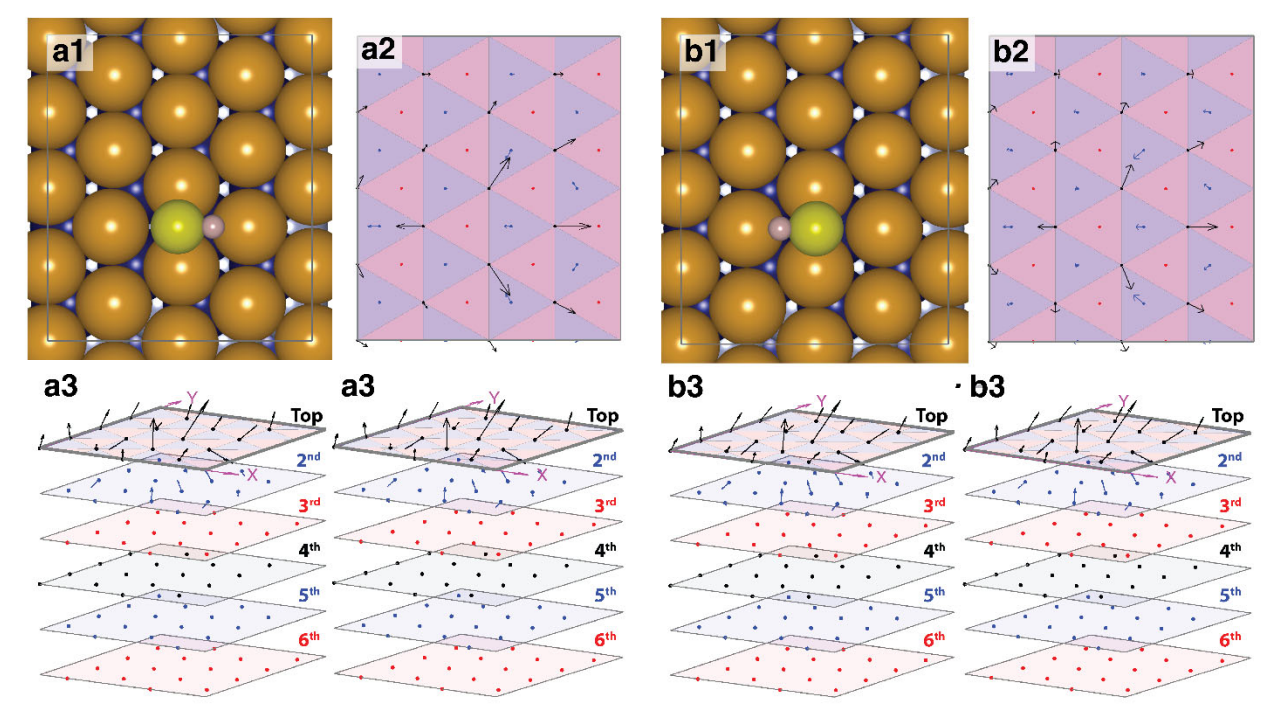


Figure S4. The Au atom displacement for SH adsorbed at the bridge-fcc (a) and the bridge-hcp (b) sites. (a1 and b1) The top-down view showing the atomic position for the adsorbates on the surface. (a2-a3 and b2-b3) Arrows represent the deviation of the Au atoms compared to their ideal unrelaxed position. The arrow length is magnified 10× for visualization. The atoms are shown in their unrelaxed position with the displacement vectors originating from their unrelaxed positions. (a2 and b2) Top-down views showing the top three Au layers and their in-plane displacement vectors. The top layer atoms (black) are at the vertices of the 3-fold-hollow-site triangles. The second layer atoms (blue) are below the hcp 3-fold hollow sites (blue triangles) and the third layer atoms (red) are below the fcc-3-fold hollow sites (red triangles). (a3 and b3) Parallel-view stereo pairs showing all the layers with their relaxation vectors in 3D.

Table S2. Comparison of the energy of the system with respect to SH (S-H, bridge-hcp) on bulk Au.

System (energy reference: SH bridge-hcp on bulk Au)	ΔE (meV)
SH(S-H, bridge-hcp) + unrelaxed Au	0
SH(S-H, bridge-fcc) + unrelaxed Au	-7.4752
SH(S-H, bridge-hcp) + relaxed Au	-293.2137
SH(S-H, bridge-fcc) + relaxed Au	-299.4319

Table S3. Displacement (Å) for the top two Au layers from the relaxed bare Au positions.

System (coordinate reference: relaxed Au)	layer	\overline{x} (Å)	$\bar{y}(\text{Å})$	\overline{z} (Å)
CH(C H builded for) An	Top layer	0.0384	0	0.0115
SH(S-H, bridge-fcc)+Au	2 nd layer	-0.0272	0	0.0066
CH(C H haider han) An	Top layer	0.0547	0	0.0126
SH(S-H, bridge-hcp)+Au	2 nd layer	-0.0260	0	0.0067
Doiles for an asless Ass	Top layer	0.0605	0	0.0147
Bridge-fcc on relax Au	2 nd layer	-0.0247	0	0.0070
Duides han an malay Ay	Top layer	0.0324	0.0072	0.0144
Bridge-hcp on relax Au	2 nd layer	-0.0266	0.0016	0.0072

Note that, the out-of-plane displacement for the 2nd layer with respect to the relaxed bare Au is larger than the unrelaxed Au. This is because the 2nd layer of the relaxed bare Au moves closer to the 3rd layer, whereas it moves away from the 3rd layer with the adsorbate during relaxation (See also Table S4).

Table S4. Displacement (Å) for the top two Au layers from their unrelaxed positions.

System	layer	\overline{x} (Å)	$\bar{y}(\text{Å})$	\overline{z} (Å)
Delayed home Av. summeloyed Av.	Top layer	0.0002	0	0.0571
Relaxed bare Au – unrelaxed Au	2 nd layer	0.0202	0.0001	-0.0058
SH(S-H, bridge-fcc)+Au – unrelaxed Au	Top layer	0.0386	0	0.0686
Sh(S-n, bhage-icc)+Au – uilleiaxeu Au	2 nd layer	-0.0070	0	0
CH(C H 1 : 1 1) I A	Top layer	0.0549	0	0.0697
SH(S-H, bridge-hcp)+Au – unrelaxed Au	2 nd layer	-0.0058	0	0
Bridge-fcc on relax Au – unrelaxed Au	Top layer	0.0608	0	0.0718
Bridge-ice on relax Au – unietaxed Au	2 nd layer	-0.0045	0	0.0011
Did a law and a Area and a Area	Top layer	0.0326	0.0072	0.0715
Bridge-hcp on relax Au – unrelaxed Au	2 nd layer	-0.0064	0.0017	0.0013

Table S5. Geometric parameters of the SH and SCH₃ adsorbates. The values in the square brackets are for the relaxed adsorbate on unrelaxed Au.

	SH(X = H)		SCH ₃	(X = C)
	bridge-fcc+Au	bridge-hcp+Au	Bridge-fcc+Au	Bridge-hcp+Au
S-top layer(Å)	2.03 [2.10]	2.06 [2.11]	1.99 [2.06]	2.03 [2.07]
S-Au _I (Å)	2.47 [2.55]	2.48 [2.56]	2.44 [2.52]	2.45 [2.52]
S-Au ₂ (Å)	2.47 [2.55]	2.48 [2.56]	2.44 [2.52]	2.45 [2.54]
Au ₁ -Au ₂ (Å)	3.12 [2.89]	3.07 [2.89]	3.14 [2.89]	3.10 [2.89]
Au_2 -S- Au_1 (°)	78.28 [68.91]	76.35 [68.76]	79.83 [69.77]	78.54 [69.57]
S-X, surface normal (°)	75.63 [77.97]	79.04 [78.06]	59.44 [59.76]	58.71 [60.25]
Au ₁ -S-X(°)	97.71 [98.18]	98.18 [97.23]	106.84 [110.08]	108.05 [108.72]
Au ₂ -S-X(°)	97.71 [98.18]	98.18 [97.23]	106.84 [110.08]	108.76 [109.91]

E. Testing the Deviation from Bridge-Site Mirror Plane Symmetry of the Bridge-hcp Site Au Surface Relaxation

The initial enforced symmetric structure for the bridge-hcp is prepared from the coordinates of the relaxed bridge-hcp system, Figure 4.b. Displacement of the mirror symmetric Au atom pairs about the bridge-site mirror plane (y coordinates) are averaged and assigned to both atoms of each pair (Figure S5.a). The calculation was then repeated, and the result shown in Figure S5.b.

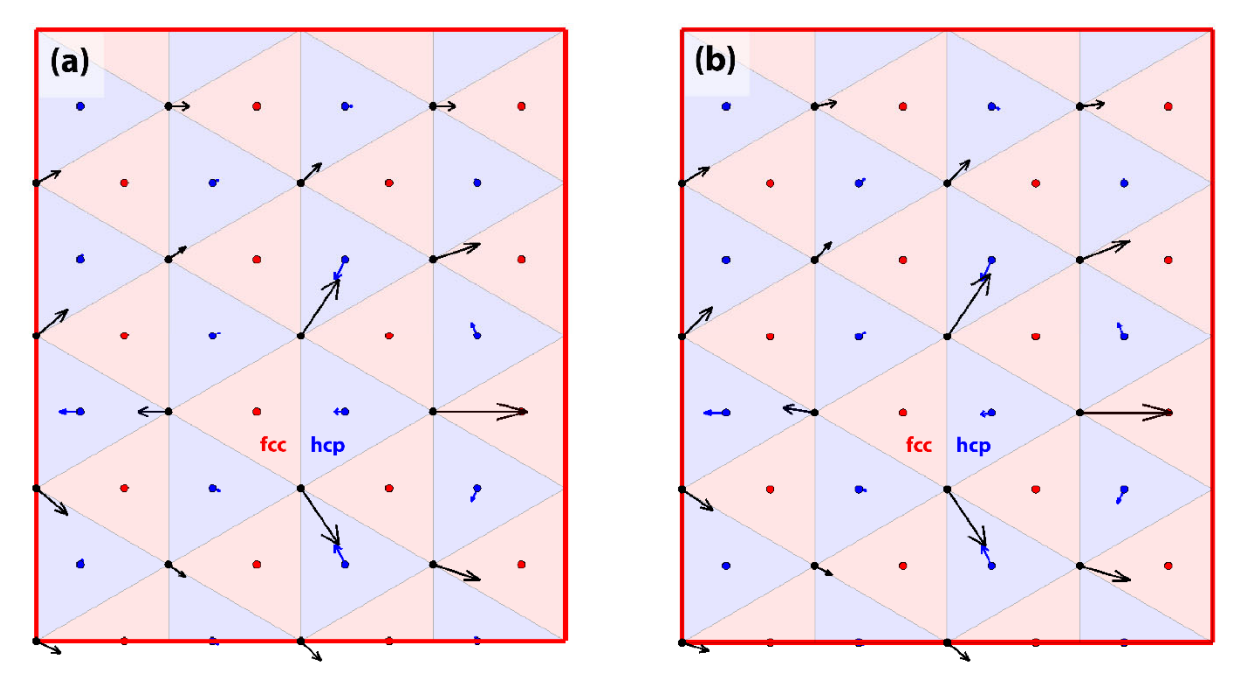


Figure S5. Initial enforced symmetric structure (a) and the subsequent relaxed structure (b) of the bridgehcp is shown. The displacement arrows are magnified by ten times for visualization.

F. References

1. Nix, F. C.; MacNair, D., The Thermal Expansion of Pure Metals: Copper, Gold, Aluminum, Nickel, and Iron. *Phys. Rev.* 1941, *60* (8), 597-605.